Published in final edited form as:
Magn Reson Med. 2013 December ; 70(6): . doi:10.1002/mrm.24616.

3D-Mapping of Phosphocreatine Concentration in the Human Calf Muscle at 7T: Comparison to 3T

Prodromos Parasoglou[1], **Ding Xia**[1], **Gregory Chang**[1], and **Ravinder R. Regatte**[1]

[1]Quantitative Multinuclear Musculoskeletal Imaging Group (QMMIG), Center for Biomedical Imaging, Department of Radiology, New York University Langone Medical Center, New York, NY, USA

Abstract

Purpose—The development and implementation of a spectrally selective 3D-Turbo Spin Echo sequence for quantitative mapping of phosphocreatine concentration in different muscles of the lower leg of healthy volunteers both at 3T and 7T.

Methods—Nine healthy volunteers were recruited, all of whom where scanned at 3T and 7T. Three dimensional phosphocreatine concentration maps were obtained after images were corrected for B_1 inhomogeneities, T_1 relaxation weighting, and partial volume of fatty tissue in the muscles. Two volunteers performed plantar flexions inside the magnet, and the oxidative capacity of their muscles was estimated.

Results—Three dimensional phosphocreatine concentration maps were obtained, with full muscle coverage and nominal voxel size of 0.52 mL at both fields. At 7T a 2.7 fold increase of signal-to-noise ratio was achieved compared to 3T.

Conclusion—Imaging ^{31}P metabolites at 7T allowed for significant increase in SNR compared to imaging at 3T, while quantification of the phosphocreatine concentration remained unaffected. The importance of such an increase in SNR is twofold, first higher resolution images with reduced partial volume effects can be acquired, and second multiple measurements such as dynamic imaging of phosphocreatine post exercise, ^{31}P magnetization transfer, or other ^{1}H measurements, can be acquired in a single imaging session.

Keywords

TSE imaging; ^{31}P imaging; calf muscle; phosphocreatine; high field ^{31}P-MRI

INTRODUCTION

In vivo Phosphorus Magnetic Resonance Spectroscopy (^{31}P-MRS) can be used to non-invasively assess bioenergetics and metabolism of skeletal muscle. The detection of metabolites that play key roles in metabolism is an important feature of ^{31}P-MRS, which has been used for over three decades to study healthy and diseased metabolic states in humans (1–13). The large chemical shift dispersion (~ 30 ppm) of ^{31}P, together with its 100% natural abundance, results in high spectral resolution even at low field strengths (14).

The vast majority of ^{31}P-MRS studies have been performed with the use of small surface coils that are placed over the muscle of interest that acquire spectra from the entire sensitive

Correspondence to: Prodromos Parasoglou, PhD, Center of Biomedical Imaging, Department of Radiology, NYU Langone Medical Center, 660 First Avenue (4th floor), New York, NY 10016, Tel: +1-212-263-2700, Fax:+1-212-263-7541, prodromos.parasoglou@nyumc.org.

area of the coil (10). Such techniques result in the acquisition of high signal to noise ratio (SNR) data that, however, provide coarse spatial resolution and limited coverage of the muscle. It is well established that most human muscles are composed of a mixture of fibre types, hence when the volume of the examined tissue is large the data usually include signals from a heterogeneous mixture of fibre types (15). Furthermore, certain diseases such as type 2 diabetes, are known to result in spatially heterogeneous alteration of the metabolic activity in the skeletal muscles (16). In order to study the propagation of such diseases and even evaluate the efficacy of interventions it would be beneficial to develop new non-invasive tools to map the metabolic activity in large areas of the muscle with relatively high spatial resolution. Therefore, successful mapping of the metabolic activity of skeletal muscle, with the use of new ^{31}P-MRI methods could become a powerful approach for the study of metabolic diseases affecting skeletal muscle, which have a rapidly increasing socioeconomic impact on both the young and the elderly.

Imaging of larger areas of the skeletal muscle can be achieved with the use of a combination of spectrally selective pulse sequences and volume radiofrequency (RF) coils (17–21). Such techniques can result in images with voxel sizes significantly smaller than those obtained with ^{31}P-MRS methods in clinically relevant acquisition times (22). Previous studies have shown that ^{31}P-MRS experiments can significantly benefit from the use of an ultra high field system (i.e. 7T), with almost a three-fold increase in SNR compared to 3T(23,24). To the best of our knowledge, such comparison for ^{31}P-MRI has not been reported in the literature. Therefore, in this study we present the implementation of a spectrally selective 3D-Turbo Spin Echo (TSE) sequence for the quantitative mapping of phosphocreatine (PCr) in different muscles of the lower leg of healthy volunteers that were examined both at 3T and 7T and discuss the advantages and disadvantages of performing ^{31}P-MRI studies at high fields.

MATERIALS AND METHODS

Human Subjects

We recruited nine healthy volunteers (five female and four male, mean ± standard deviation age: 36.2 ± 11.4 yr, min/max 25/60 yr, mean ± standard deviation BMI: 24.3 ± 4.8, min/max 19.4/32.3), all of whom where scanned both on 3T and 7T MRI systems (Siemens Medical Solutions, Erlangen, Germany) using two geometrically identical dual-tuned ^{31}P/^{1}H quadrature knee coils (Rapid MRI, Ohio) with 18 cm inner diameter and 20 cm length. For each volunteer, the two scans were performed on different days. The New York University School of Medicine Institutional Review Board approved the examination protocol for the study, and all subjects provided written consent for participation in the study.

PCr Imaging with 3D-TSE

We obtained PCr images using a 3D-TSE sequence (described in our previous work (22)) that we developed using the ‘SequenceTree’ software (25). In our sequence, the 90° excitation pulse is narrowband Gaussian with 8 ms duration at 7T (theoretical bandwidth: 250 Hz), and 16 ms duration at 3T (theoretical bandwidth 125 Hz). Previously, we had experimentally measured the actual excitation bandwidth of the pulse at 122 Hz (3T) and 220 Hz (7T) (26). The excitation pulse is applied without the use of a slice selective gradient. After each spectrally selective excitation, acquisition starts at (or close to) the centre of the primary phase encoding direction (y-direction), with the effective echo time at 26 ms, followed by a train (ETL) of twenty four non-selective refocusing (180°) pulses, with 26 ms echo spacing. Spin echoes are sampled with a 2.5 kHz bandwidth. It has been shown previously that the signals of the ATP ^{31}P resonances after excitation modulate both in amplitude and phase due to J-coupling among the individual resonances of that molecule

(27,19). For the case of multi-echo sequences (such as the TSE employed in this study), ATP signals cancel out when the echo-spacing is set to 26 ms, hence minimizing any contamination of the PCr signal from off-resonance excitation of ATP.

We obtained images with field-of-view (FOV) of 220 × 220 × 200 mm to avoid any wrap-around artifacts due to the lack of slice selective gradients, with matrix size of 48 × 48 × 8, yielding a nominal voxel size of 0.52 mL, with TR = 12 s, and scan time of 3 min and 12 s per signal average. At 7T we acquired 3 averages (10 min acquisition time), while at 3T we acquired 5 averages (16 min acquisition time). We calculated the SNR of the PCr images as the mean signal intensity of the entire calf muscle divided by the standard deviation of the noise.

Calibration phantom images with comparable coil loading were acquired using the same pulse sequence at fully relaxed conditions (TR = 60 s). The phantom was used to derive the calibration curve of PCr as a function of signal intensity. The phantom consisted of two sealed cylindrical tubes containing different inorganic phosphate concentrations (25 and 50 mM).

Apparent T_1 mapping with 3D-IR-TSE

The imaging sequence described above was slightly modified in order to measure the apparent T_1 of PCr in the muscles of the lower leg by adding an inversion pulse to the 3D-TSE sequence. An adiabatic Wideband, Uniform Rate, and Smooth Truncation (WURST) shape pulse was used for inversion (28), with 5 ms duration and 250 Hz bandwidth at 7T and 125 Hz at 3T. At 7T, eight images were acquired at inversion times (TI) of 200, 700, 1000, 1800, 3000, 5000, 8000, 15000 ms, with 24 × 24 × 8 matrix size (zero-filled to 48 × 48 × 8 prior to reconstruction), and TR = 15 s. At 3T, seven images were acquired with 16 × 16 × 8 matrix size (zero-filled to 48 × 48 × 8 prior to reconstruction), TR = 30 s, TI: 200, 1500, 3000, 6000, 10000, 15000, 20000 ms. In both fields, images were acquired with the same FOV and frame of reference as the PCr images described above. The total acquisition time for the apparent T_1 measurement was 18 min at 7T and 33 min at 3T.

B_1 Mapping

We mapped RF inhomogeneities of the ^{31}P channel of both coils using the Actual Flip-Angle Imaging (AFI) method (29). At 7T, we acquired images with TR_1 = 500 ms, TR_2 = 3500 ms, and 24 × 24 × 8m matrix size. At 3T, we acquired images with TR_1 = 800 ms, TR_2 = 4500 ms, and 16 × 16 × 8 matrix size. At both fields, the nominal flip angle was 60° with the same FOV and frame of reference as the PCr images. By dividing the two images, we calculated the actual to nominal flip angle ratio (r) for each voxel. The acquisition time of the B_1 mapping sequence was 11 min at 3T and 12 min at 7T, and was included as part of the imaging protocol for each subject. The images in both fields were zero-filled to 48 × 48 × 8 prior to reconstruction.

^{1}H Imaging

To verify muscle anatomy, we used two product sequences (i.e. a gradient echo [GRE] sequence and a TSE sequence). All 3D-^{1}H images were acquired with the same FOV and frame of reference as the PCr images, with matrix size of 128 × 128 × 40.

Dynamic Imaging of PCr Resynthesis

We collected PCr images during and after exercise in two of the recruited subjects during the 7T scan. The participants performed plantar flexions using resistance bands for 2 min, at a frequency of 1 repetition per second. Images were acquired using a compressed sensing 3D-TSE technique with 2-fold acceleration, 12 s temporal resolution and 2.1 mL nominal

voxel size that we described previously (30). Images were acquired with the same FOV and frame of reference as the resting PCr images. It is important to note, that the physical exercise was designed to decrease PCr without inducing acidosis, thus avoiding pH effects on mitochondrial ATP synthesis (26). The total time of the experiment was 10 min.

PCr Quantification

Prior to estimation of the apparent T_1 values in the muscles, images acquired at different TIs were corrected for B_1 inhomogeneities by normalizing the signal intensities using the following equation (31):

$$f_1=\frac{\sin(r\cdot 90)[1-\cos(r\cdot 180)]}{2[1-\cos(r\cdot 90)\cos(r\cdot 180)]} \quad [1]$$

While PCr images were corrected for B_1 inhomogeneities and T_1 relaxation weighting using the following correction:

$$f_2=\frac{1-E_1}{2}\frac{\sin(r\cdot 90)[1-\cos(r\cdot 180)]}{[1-E_1\cos(r\cdot 90)\cos(r\cdot 180)]} \quad [2]$$

where $E_1 = \exp(TR/T_1)$. Signal intensities of the corrected PCr images were compared voxel-wise to the calibration line obtained from the phantoms to extract PCr concentration maps ([PCr]). These concentrations are in mmol/L tissue and can be converted to mmol/L cell water (mM) through multiplication by a conversion factor (in this case equal to 1.41) that takes into account the water content of the muscle (32).

Obese subjects (BMI > 30) can have some fat in the muscle tissue. In addition, many muscle weakening and metabolic disorders lead to an increase in adipose tissue in and around the muscles, which will drastically influence PCr quantification, if not accounted for. Thus, a measurement of absolute PCr concentration in muscle tissue mustinclude a method to correct for partial volume of the fatty tissue in those cases. In order to determine the volume fraction of fat/muscle in the tissue, we used high-resolution ^{1}H images to segment the fat in the case of an obese male subject (BMI = 32.3). The binary images of the muscle (matrix size 128 × 128 × 40) were downsampled to the size of the PCr images (i.e. 48 × 48 × 8), using linear interpolation, which resulted in an estimate of the muscle volume fraction (n_m) in the PCr images. The muscle volume fraction was used to correct signal intensity and account for the presence of fat.

A flowchart of the data acquisition and PCr quantification process is shown in Fig. 1.

Oxidative Capacity Measurement

Skeletal muscle oxidative capacity was determined from the kinetics of PCr recovery after a 2-minute plantar flexion exercise. For each of the two participants, rate constants (k_{PCr}) of PCr recovery were determined by fitting a single exponential curve to segmented volumes of interest (VOIs) in different muscles:

$$PCr(t)=\Delta PCr[1-\exp(-k_{PCr}t)]+PCr_{ex} \quad [3]$$

Where t is the time, PCr_{ex} is [PCr] at the end of exercise, $\Delta PCr = PCr_{rest} - PCr_{ex}$ (10,33), with PCr_{rest} measured through the static experiment described previously. Oxidative capacity (Q_{max}, mM ATP s^{-1}) was determined as the product of k_{PCr} and PCr_{rest}.

RESULTS

Phosphorus B_1 maps for a central slice of one of the volunteers are shown in Fig. 2. At 3T (right) the actual to nominal flip angle ratio (r) is close to 1 in the entire slice, while at 7T larger variations are observed. Corrections of RF field inhomogeneities were applied in the signal intensities of images acquired at different TIs (through Eq. 1) prior to T_1 fitting, and to PCr images prior to [PCr] mapping through Eq. 2.

Apparent T_1 values were measured for each volunteer at 3T and 7T, using inversion recovery (IR)-3D-TSE. A series of seven images acquired at different inversion times (TI) are shown in Fig. 3a. At 7T, eight images were acquired for the same volunteer (Fig. 3b). An example of T_1 fitting in the tibialis anterior muscle of the volunteer is shown in Fig. 3d. In this case apparent T_1 was measured at 5.82 s at 3T, with a 38% reduction (3.61 s) at 7T. The mean ± standard deviation of the apparent T_1 values measured in the different muscles of the lower leg of the volunteers are summarized in Table 1. The abbreviations used for the different muscles of the lower leg are: GL: Gastrocnemius medial head, Gastrocnemius lateral head, P: Peroneus (brevis and longus) S: Soleus, TA: Tibialis Anterior, TP: Tibialis Posterior. The average decrease of apparent T_1 at 7T was 39% compared to 3T.

We acquired PCr images with three signal averages at 7T, yielding an average SNR of 24.3 ± 2.5, while five signal averages at 3T resulted in SNR of 11.5 ± 0.8 (8.9 ± 0.6 for three averages). Therefore, for the same number of averages, a close to 2.7 fold increase was observed at 7T relative to 3T for the same nominal resolution. After correcting the signal intensity and comparing it to the calibration curve, we obtained [PCr] maps, an example of which is shown in Fig. 4 for a female volunteer at 3T and 7T, along with the anatomical ^{1}H images. In the absence of adipose tissue in the muscle, [PCr] mapping can be performed by assuming constant water content in the muscle. In the presence of fat in the muscle tissue, this assumption can lead to underestimation of the [PCr]. An example of a male subject with BMI = 32.3 is shown in Fig. 5 (top left). By assuming constant water content in the muscle, big fluctuations in [PCr] maps can be observed (bottom left). These fluctuations show decreased [PCr] in voxels where there is more fat, as shown in the overlaid image (middle). To correct for the fraction of muscle and fat in a volume of interest, segmentation of the fat can be used (top right), which, after downsampling it to the size of the PCr image (i.e. 48 × 48 × 8), can give a measure of the fraction of muscle and fat in the voxels. This muscle fraction provides an estimate of the actual content within a segmented volume of interest (VOI), and is correcting the [PCr] within the VOI.

Resting [PCr], together with the rate constant (k_{PCr}) of PCr recovery following exercise, can be used to estimate the oxidative capacity in skeletal muscle. An example of resting [PCr] map of a 60 yr old female volunteer is shown in Fig 6. a. Following exercise, [PCr] levels are depleted in the tibialis anterior muscle, as can be seen in Fig. 6b. After sufficient time, [PCr] levels return to the resting values. By segmenting a VOI within the tibialis anterior we plotted the PCr resynthesis Fig. 6c and fitted Eq. 3 to the data. In this example, k_{PCr} was measured at 0.027 s^{-1}. In addition, the oxidative capacity (Q_{max}) in the TA muscle of this volunteer was measured at 0.69 mM ATP s^{-1}.

DISCUSSION

We have demonstrated the feasibility of acquiring [PCr] maps in large volumes of the lower leg muscles, both at 3T and 7T with nominal voxel size of 0.52 mL at both fields. This is important, because [PCr] maps are required in order to measure oxidative capacity in different muscles of healthy and diseased subjects, as well as metabolic fluxes using magnetization transfer (MT) imaging experiments. In this work, we observed a 2.7-fold

increase in SNR at 7T compared to 3T, which is consistent with SNR increase observed in ^{31}P-MRS studies (24). Higher SNR at 7T, allowed for acquisition of higher resolution apparent T_1 maps and B_1 maps. At the same time, the decrease of apparent T_1 at 7T, allowed for faster T_1 measurements using shorter TR (15 s at 7T, compared to 30 s at 7T). Mapping of PCr concentration in several muscles of the lower leg using surface coils, would require repositioning of the coil and repetition of the experiment several times in order to provide a similar coverage of the muscle to our methods.

It can be argued that imaging of a single metabolite of the ^{31}P spectrum (i.e. PCr) lacks important information about intracellular pH, inorganic phosphate (Pi) and ATP that are readily available with MRS acquisitions, normally performed in coarser volumes of the muscle with the use of surface coils. It is important to note, however, that there are very important studies currently performed with unlocalized MRS methods that rely on the measurement of the PCr peak alone. Benerjee and co-workers (13) studied the efficacy of creatine supplementation in ambulatory Duchenne muscular dystrophy patients using unlocalized ^{31}P-MRS, by monitoring the increase of PCr longitudinally. Such studies can be performed using our method, in order to understand the spatial variability of the disease propagation and the progress of the treatment. Moreover, ^{31}P magnetization transfer (MT) experiments, which provide information about the steady state metabolite turnover, therefore reflecting mitochondrial activity are also performed with unlocalized ^{31}P MRS (10,34). Such measurements rely on the measurement of the PCr signal when metabolites that are chemically exchanging (i.e. Pi and ATP) are saturated. Hence, it is possible to spatially map the PCr signal with and without saturation of the chemically exchanging moiety with our method by adding an MT preparation module. For absolute quantification of the metabolic fluxes, in order to compare data between subjects, mapping of the baseline concentration of PCr is required, which is the subject of the current work. Finally, as we showed here imaging of the dynamic recovery of PCr post exercise, is also possible using a similar imaging method with a temporal resolution of 12 s, which is using the resting [PCr] in order to quantify oxidative capacity in muscle. The oxidative capacity measurements obtained in this study, although in need of replication, are well within the range reported in the literature measured with ^{31}P-MRS (35,36).

One of the limitations of our work is that [PCr] maps are extracted without accounting for local T_2 variations. These local variations in T_2 will increasingly affect PCr quantification when images are heavily T_2 weighted. Our method is using a centric k-space sampling pattern with effective echo time of 26 ms that minimizes T_2 weighing in voxels. At this effective echo time, using localized T_2 values reported in the literature (23), we expect a maximum of 0.5% error introduced in the 3T measurement and 6% error at 7T due to the lack of T_2 mapping. It is important to note, that T_1 values measured for PCr in this study are not the true longitudinal relaxation times, but rather apparent T_1 values, since PCr undergoes chemical exchanges with other metabolites (37). True T_1 rates can be measured with magnetization transfer experiments, taking into account the chemical exchange rates between the different metabolites. Compared to previously reported apparent T_1 values in the calf muscle, our measurements appear to be systematically lower. Using localized ^{31}P-MRS methods at 3T, El-Sharkawy *et al.* (38), reported mean T_1 values of 6.8 s, while Meyerspeer *et al.* (39) reported mean T_1 values of 6.4 s. Bogner *et al.* (23), used unlocalized ^{31}P-MRS and measured mean T_1 values of 6.7 s. In this work, using ^{31}P-MRI, we measured mean T_1 values in different muscles that range between 5.8 and 6.1 s (Table 1). Similarly, at 7T Bogner *et al.* (23), reported T_1 values of 4.0 s, while our measurements in the different muscle range between 3.5 and 3.6 s. There are several instrumental factor that can introduce errors in T_1 measurements, especially when acquired in an imaging context. T_1 measurements, assume ideal 90° and 180° pulses; in the case of imaging experiments there are several sources of spatially-dependent systemic errors in the RF pulse

angle due to non-uniform RF irradiation, and hence in the measured relaxation times (40). In addition, whenever narrowband excitation pulses are used (such as the spectrally-selective Gaussian pulses used in our method), the RF profiles of those pulses can introduce additional errors to measured T_1 values (41).

In our exiting protocol, quantification of PCr requires the acquisition of several measurements (i.e. PCr imaging, B_1 mapping, T_1 mapping, and ^{1}H anatomical imaging). The total acquisition time at 3T is 62 min, while at 7T it is 42 min. There are different challenges in the quantification process of PCr concentration at 3T and 7T. At 3T, B_1 inhomogeneities are less severe compared to 7T (as can be seen in Fig. 2). Therefore, omitting B_1 measurements can reduce the total experimental time at 3T by 11 min, resulting in a 53 min acquisition. At 7T, with a TR of 12 s and T_1 in the muscles close to 3.5 s (Table 1), there is very little T_1 weighing in the images (less than 5%), and therefore localized T_1 measurements can be omitted, or replaced by faster, unlocalized measurements, which can reduce the acquisition time to 24 min. In both cases, all measurements can be performed within one imaging session which typically lasts 60 min. However, at 7T the increase in SNR and the reduction in T_1 values can allow for faster (by a factor of two) acquisitions.

The results presented in this study show that imaging ^{31}P metabolites at 7T allows a significant (almost threefold) boost in SNR compared to imaging at 3T, while quantification of the PCr concentration remains unaffected. This increase is larger than the increase in ^{1}H studies (close to twofold) due to the chemical shift anisotropy effect in the case of ^{31}P (42). The importance of such an increase in SNR is twofold, first higher resolution images with reduced partial volume effects can be acquired, and second multiple measurements (i.e. dynamic imaging of PCr, MT, or other ^{1}H measurements) can be acquired in a single imaging session, which typically lasts between 45 and 60 min.

Acknowledgments

Grant sponsor: The authors would like to acknowledge the support by research grants RO1 AR053133, RO1 AR056260, and RO1 AR060238 from the National Institute of Arthritis and Musculoskeletal and Skin Diseases (NIAMS), National Institutes of Health (NIH).

This research work was partly supported by National Institutes of Health grants R01-AR053133, R01-AR050260 and R01-AR060238

References

1. Chance B, Eleff S, Leigh JS. Non-invasive, non-destructive approaches to cell bioenergetics. Proc Natl Acad Sci USA. 1980; 77(12):7430–7434. [PubMed: 6938983]
2. Chance B, Eleff S, Leigh JS, Sokolow D, Sapega A. Mitochondrial regulation of phosphocreatine inorganic-phosphate ratios in exercising human-muscle- a gated 31P NMR study. Proc Natl Acad Sci USA. 1981; 78(11):6714–6718. [PubMed: 6947247]
3. Newman RJ, Bore PJ, Chan L, Gadian DG, Styles P, Taylor D, Radda GK. Nuclear magnetic-resonance studies of forearm muscle in Duchenne dystrophy. Brit Med J. 1982; 284(6322):1072–1074. [PubMed: 6802410]
4. Bottomley PA, Charles HC, Roemer PB, Flamig D, Engeseth H, Edelstein WA, Mueller OM. Human invivo phosphate metabolite imaging with 31P NMR. Magn Reson Med. 1988; 7(3):319–336. [PubMed: 3205148]
5. Miller RG, Boska MD, Moussavi RS, Carson PJ, Weiner MW. 31P nuclear magnetic resonance studies of high-energy phosphates and pH in human-muscle fatigue-comparison of aerobic and anaerobic exercise. J Clin Invest. 1988; 81(4):1190–1196. [PubMed: 3350969]
6. Bottomley PA, Hardy CJ, Roemer PB. Phosphate metabolite imaging and concentration measurements in human heart by nuclear magnetic resonance. Magn Reson Med. 1990; 14(3):425–434. [PubMed: 2355826]

7. Dunn JF, Kemp GJ, Radda GK. Depth selective quantification of phosphorus metabolites in human calf muscle. NMR Biomed. 1992; 5(3):154–160. [PubMed: 1642973]
8. Kemp GJ, Taylor DJ, Radda GK. Control of phosphocreatine resynthesis during recovery from exercise in human skeletal-muscle. NMR Biomed. 1993; 6(1):66–72. [PubMed: 8457428]
9. Doyle VL, Payne GS, Collins DJ, Verrill MW, Leach MO. Quantification of phosphorus metabolites in human calf muscle and soft-tissue tumours from localized MR spectra acquired using surface coils. Phys Med Biol. 1997; 42(4):691–706. [PubMed: 9127445]
10. Prompers JJ, Jeneson JAL, Drost MR, Oomens CCW, Strijkers GJ, Nicolay K. Dynamic MRS and MRI of skeletal muscle function and biomechanics. NMR Biomed. 2006; 19(7):927–953. [PubMed: 17075956]
11. Haseler LJ, Lin A, Hoff J, Richardson RS. Oxygen availability and PCr recovery rate in untrained human calf muscle: evidence of metabolic limitation in normoxia. Am J Physiol-Reg I. 2007; 293(5):R2046–R2051.
12. Phielix E, Mensink M. Type 2 diabetes mellitus and skeletal muscle metabolic function. Physiol Behav. 2008; 94(2):252–258. [PubMed: 18342897]
13. Banerjee B, Sharma U, Balasubramanian K, Kalaivani M, Kalra V, Jagannathan NR. Effect of creatine monohydrate in improving cellular energetics and muscle strength in ambulatory Duchenne muscular dystrophy patients: a randomized, placebo-controlled (31)P MRS study. Magn Reson Imaging. 2010; 28(5):698–707. [PubMed: 20395096]
14. de Graaf, RA. Vivo NMR Spectroscopy. John Wiley & Sons, Ltd; Chichester: 2007. Front Matter.
15. Taylor DJ. Clinical utility of muscle MR spectroscopy. Seminars in musculoskeletal radiology. 2000; 4(4):481–502. [PubMed: 11371330]
16. Oberbach A, Bossenz Y, Lehmann S, Niebauer J, Adams V, Paschke R, Schon MR, Bluher M, Punkt K. Altered fiber distribution and fiber-specific glycolytic and oxidative enzyme activity in skeletal muscle of patients with type 2 diabetes. Diabetes Care. 2006; 29(4):895–900. [PubMed: 16567834]
17. Greenman RL, Elliott MA, Vandenborne K, Schnall MD, Lenkinski RE. Fast imaging of phosphocreatine using a RARE pulse sequence. Magn Reson Med. 1998; 39(5):851–854. [PubMed: 9581617]
18. Greenman RL, Axel L, Ferrari VA, Lenkinski RE. Fast imaging of phosphocreatine in the normal human myocardium using a three-dimensional RARE pulse sequence at 4 tesla. J Magn Reson Im. 2002; 15(4):467–472.
19. Greenman RL. Quantification of the P-31 metabolite concentration in human skeletal muscle from RARE image intensity. Magn Reson Med. 2004; 52(5):1036–1042. [PubMed: 15508151]
20. Greenman RL, Smithline HA. The feasibility of measuring phosphocreatine recovery kinetics in muscle using a single-shot (31)P RARE MRI sequence. Acad Radiol. 2011; 18(7):917–923. [PubMed: 21536463]
21. Greenman RL, Wang X, Smithline HA. Simultaneous acquisition of phosphocreatine and inorganic phosphate images for Pi:PCr ratio mapping using a RARE sequence with chemically selective interleaving. Magn Reson Imaging. 2011; 29(8):1138–1144. [PubMed: 21641744]
22. Parasoglou P, Xia D, Regatte RR. Spectrally selective 3D TSE imaging of phosphocreatine in the human calf muscle at 3 T. Magn Reson Med. 201210.1002/mrm.24288
23. Bogner W, Chmelik M, Schmid AI, Moser E, Trattnig S, Gruber S. Assessment of (31)P Relaxation Times in the Human Calf Muscle: A Comparison between 3 T and 7 T In Vivo. Magn Reson Med. 2009; 62(3):574–582. [PubMed: 19526487]
24. Bogner W, Chmelik M, Andronesi OC, Sorensen AG, Trattnig S, Gruber S. In Vivo (31)P Spectroscopy by Fully Adiabatic Extended Image Selected In Vivo Spectroscopy: A Comparison Between 3 T and 7 T. Magn Reson Med. 2011; 66(4):923–930. [PubMed: 21446033]
25. Magland, J.; Wehrli, FW. Pulse sequence programming in a dynamic visual environment. Proc Fourteenth Meeting Proceedings; 2006; Seattle WA. Seattle, Washington: ISMRM; p. 578
26. Parasoglou P, Xia D, Chang G, Regatte RR. Dynamic Imaging of Phosphocreatine Recovery Kinetics in the Human Lower Leg Muscles at 3T and 7T: A preliminary Study. NMR Biomed. 201210.1002/nbm.2866

27. Chao H, Bowers JL, Holtzman D, Mulkern RV. Multi-echo 31P spectroscopic imaging of ATP: A scan time reduction strategy. J Magn Reson Im. 1997; 7(2):425–433.
28. Kupce E, Freeman R. Adiabatic pulses for wide-band inversion and broad-band decoupling. J Magn Reson Ser A. 1995; 115(2):273–276.
29. Yarnykh VL. Actual flip-angle imaging in the pulsed steady state: A method for rapid three-dimensional mapping of the transmitted radiofrequency field. Magn Reson Med. 2007; 57(1):192–200. [PubMed: 17191242]
30. Parasoglou P, Feng L, Xia D, Otazo R, Regatte RR. Rapid 3D-Imaging of Phosphocreatine Recovery Kinetics in the Human Lower Leg Muscles with Compressed Sensing. Magn Reson Med. 2012; 68(6):1738–1746. [PubMed: 23023624]
31. Collewet G, Davenel A, Toussaint C, Akoka S. Correction of intensity nonuniformity in spin-echo T(1)-weighted images. Magn Reson Imaging. 2002; 20(4):365–373. [PubMed: 12165356]
32. Kemp GJ, Meyerspeer M, Moser E. Absolute quantification of phosphorus metabolite concentrations in human muscle in vivo by P-31 MRS: a quantitative review. NMR Biomed. 2007; 20(6):555–565. [PubMed: 17628042]
33. Lanza IR, Bhagra S, Nair KS, Port JD. Measurement of Human Skeletal Muscle Oxidative Capacity by P-31-MR Spectroscopy: A Cross-Validation With In Vitro Measurements. JMRI. 2011; 34(5):1143–1150. [PubMed: 22006551]
34. Valkovic L, Chmelik M, Kukurova IJ, Krssak M, Gruber S, Frollo I, Trattnig S, Bogner W. Time-resolved phosphorous magnetization transfer of the human calf muscle at 3 T and 7 T: A feasibility study. Eur J Radiol. 10.1016/j.ejrad.2011.09.024
35. Conley KE, Jubrias SA, Esselman PC. Oxidative capacity and ageing in human muscle. J Physiol (Lond). 2000; 526(1):203–210. [PubMed: 10878112]
36. Lanza IR, Larsen RG, Kent-Braun JA. Effects of old age on human skeletal muscle energetics during fatiguing contractions with and without blood flow. J Physiol (Lond). 2007; 583(3):1093–1105. [PubMed: 17673506]
37. Alger JR, Shulman RG. NMR-studies of enzymatic rates in vitro and in vivo by magnetization transfer. Q Rev Biophys. 1984; 17(1):83–124. [PubMed: 6091170]
38. El-Sharkawy A-M, Schar M, Ouwerkerk R, Weiss RG, Bottomley PA. Quantitative Cardiac P-31 Spectroscopy at 3 Tesla Using Adiabatic Pulses. Magn Reson Med. 2009; 61(4):785–795. [PubMed: 19195018]
39. Meyerspeer M, Krssak M, Moser E. Relaxation times of P-31-metabolites in human calf muscle at 3 T. Magn Reson Med. 2003; 49(4):620–625. [PubMed: 12652531]
40. Pykett IL, Rosen BR, Buonanno FS, Brady TJ. Measurement of spin-lattice relaxation-times in nuclear magnetic resonance imaging. Phys Med Biol. 1983; 28(6):723–729. [PubMed: 6878430]
41. Mansfield P, Maudsley AA, Morris PG, Pykett IL. Selective pulses in NMR imaging - Reply to criticism. J Magn Reson. 1979; 33(2):261–274.
42. Evelhoch JL, Ewy CS, Siegfried BA, Ackerman JJH, Rice DW, Briggs RW. P-31 spin-lattice relaxation-times and resonance linewidths of rat-tissue invivo - dependence upon the static magnetic-field strength. Magn Reson Med. 1985; 2(4):410–417. [PubMed: 4094555]

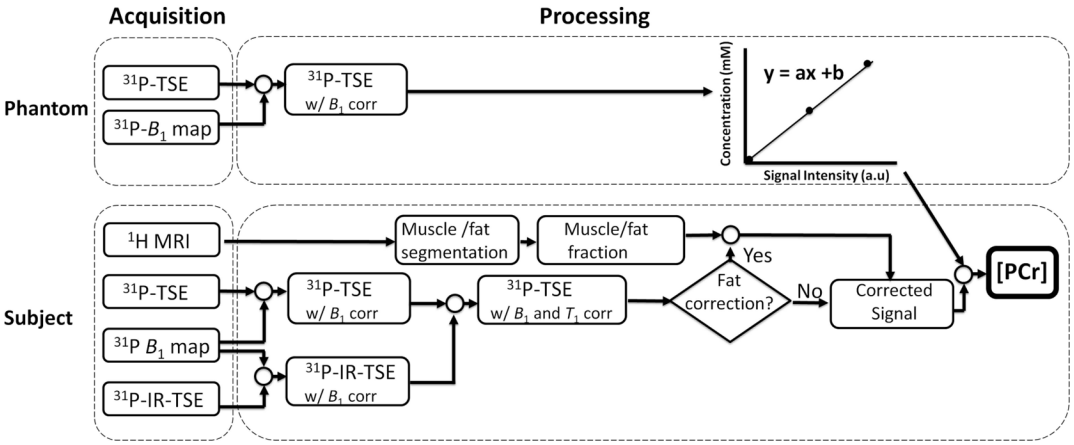

Fig. 1.

Flow chart of the data acquisition, image reconstruction and quantification processes for measuring PCr concentration in muscles of the lower leg. Inorganic phosphate phantoms are used to derive a calibration curve of PCr concentration as a function of signal intensity (top). Imaging of phantomes is performed under fully relaxed conditions (TR = 60 s), and therefore there is no T_1 correction step in the processing. In-vivo PCr images (bottom) are corrected (B_1, T_1) and compared voxelwise against the calibration curve. In cases where significant fat infiltration is present in the muscles, ^{1}H images can be used to estimate the fraction of fat/muscle in the tissue.

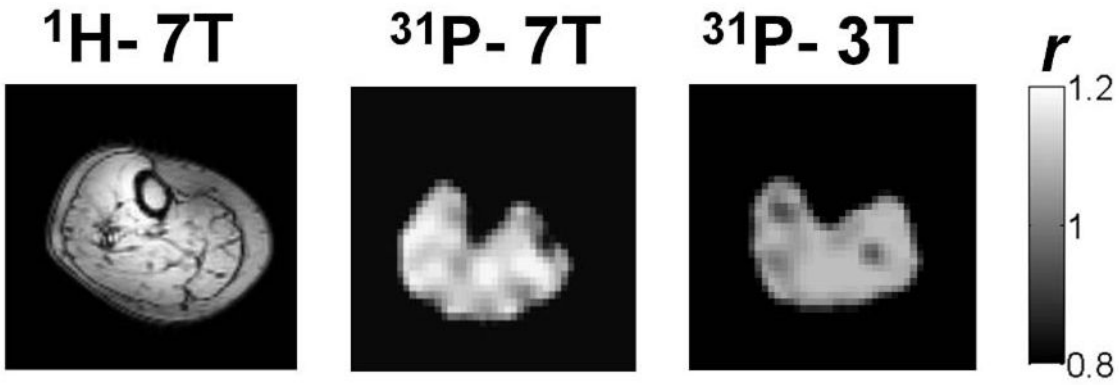

Fig. 2.
Actual to nominal flip angle maps (*r*) of the same volunteer at 3T (right) and 7T (middle) together with an anatomical ^{1}H image acquired at 7T (left).

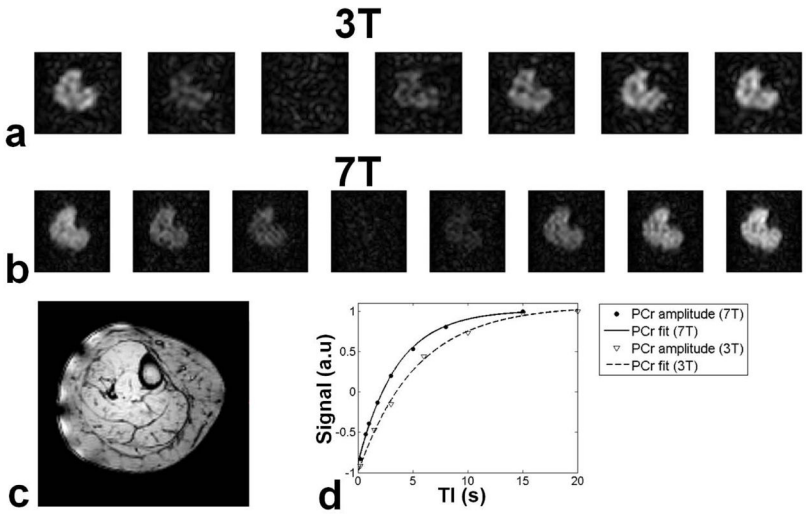

Fig. 3.

Apparent T_1 measurement of the same volunteer at 3T and 7T. a) At 3T seven images were acquired at different inversion times *TI*: 200, 1500, 3000, 6000, 10000 15000, 20000 ms. b) At 7T eight images were acquired at different *TI*: 200, 700, 1000, 1800, 3000, 5000, 8000, 15000 ms. c) Anatomical image acquired at 7T. d) T_1 fitting in the tibialis anterior (TA). At 3T apparent T_1 was 5.82 s, which reduced to 3.61 s at 7T.

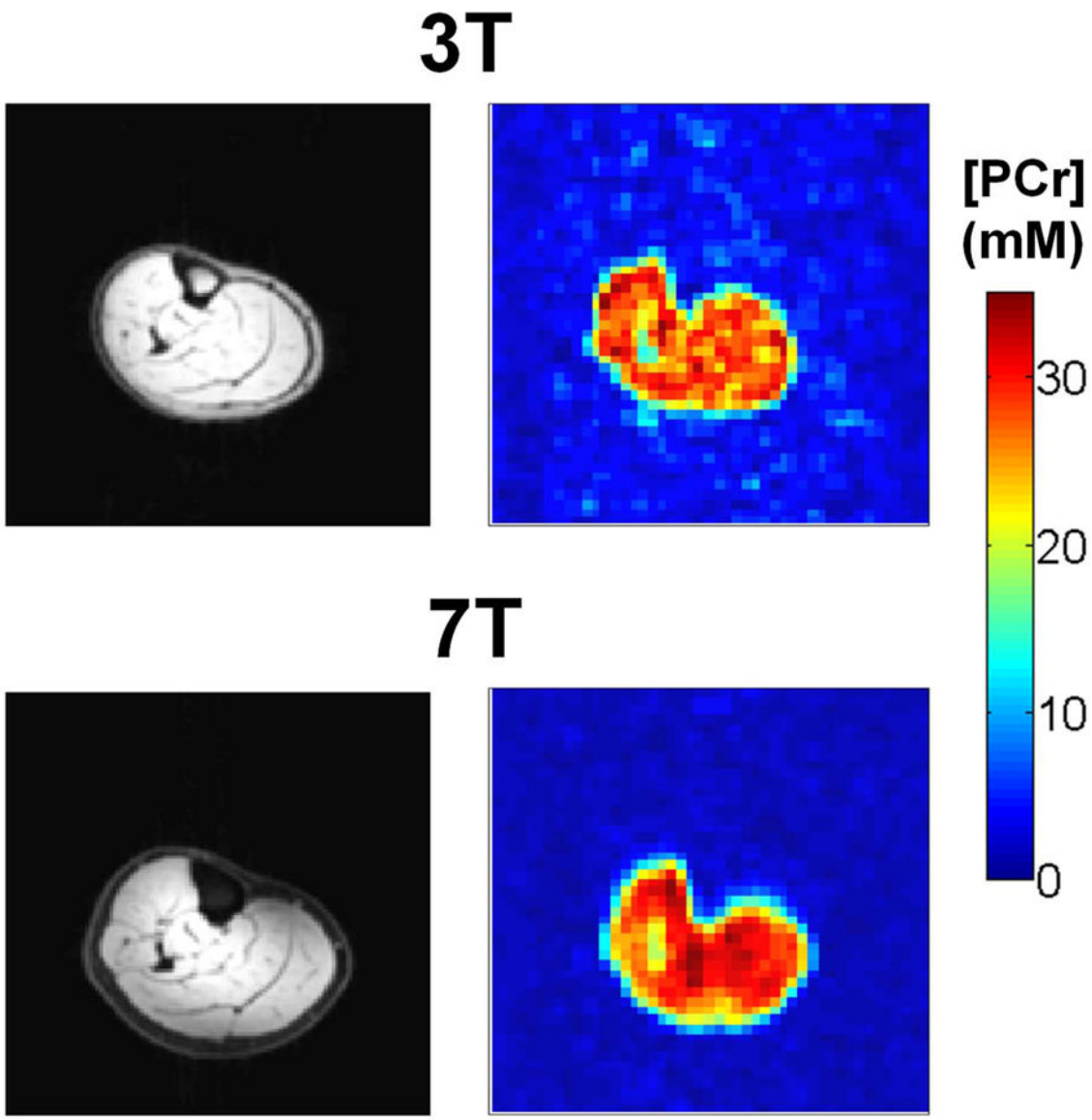

Fig. 4.
PCr concentrations maps and respective anatomical ^{1}H images at 3T (top) and 7T (bottom) from the same female volunteer after T_1 and B_1 correction. At 3T five averages where acquired (SNR = 11:1), while three signal averages at 7T yielded SNR of 25:1.

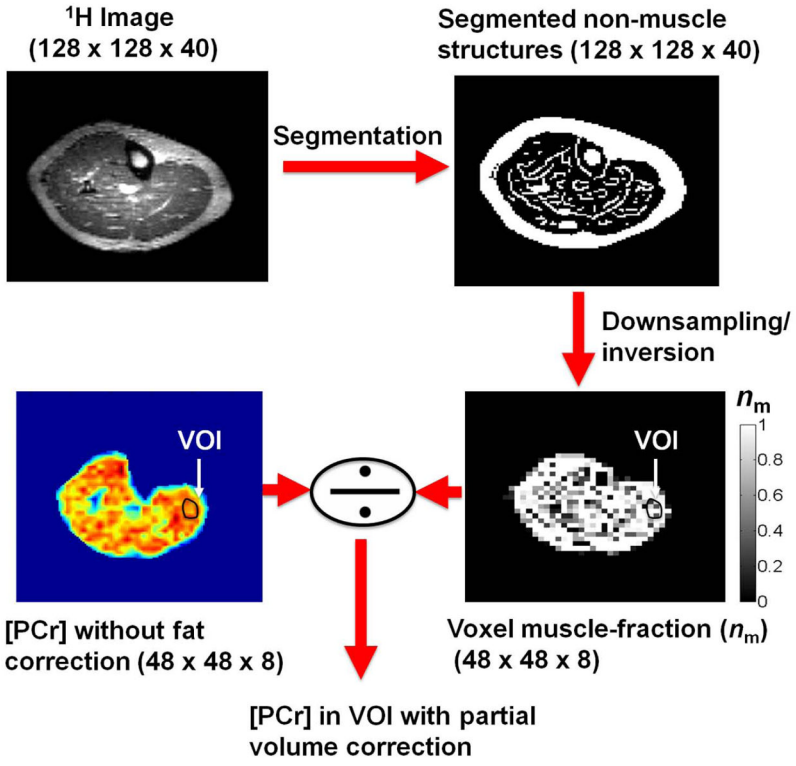

Fig. 5.

Segmentation of fat in the muscle tissue. High resolution ^{1}H datasets can be used to identify adipose tissue in the muscle (top left), that can be segmented (top right). [PCr] maps extracted without correction of fat content exhibit fluctuations (bottom left), in areas where voxels contain signals both from fat and muscle as can be seen by overlaying the ^{1}H and ^{31}P images (middle). Fat segmentations can be inverted and downsampled to the size of the PCr image, in order to estimate the muscle fraction in the voxels (n_m). By selecting a VOI, [PCr] can be extracted by correcting for partial volume effects of fat infiltration.

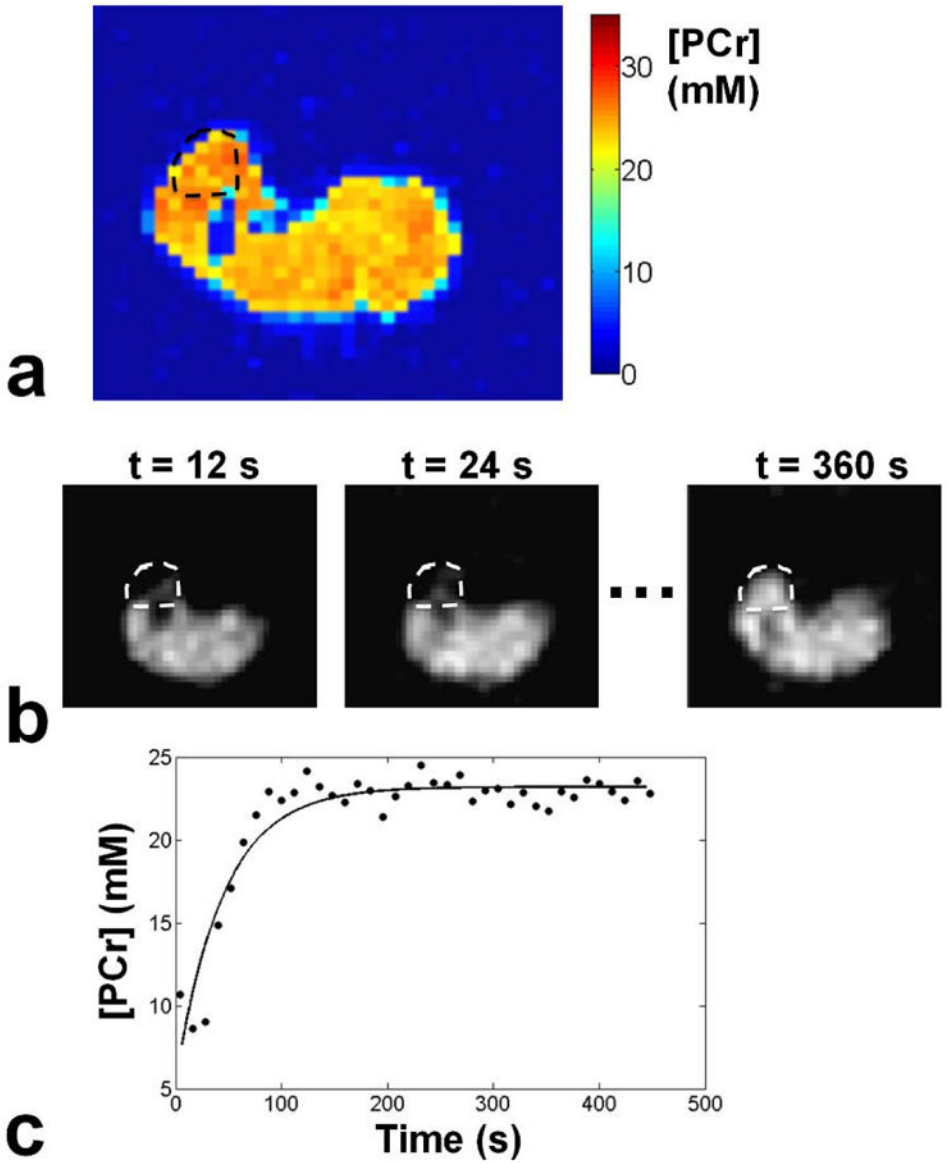

Fig. 6.

Measurement of oxidative capacity in the muscle of a 60 yr old female volunteer. a) [PCr] map at rest b) Dynamic imaging of PCr resynthesis post exercise at 12 s temporal resolution. PCr levels in the TA are depleted immediately after exercise (t = 12 s), and fully recover after sufficient time (t = 360 s). c) Evolution of [PCr] in the TA muscle post-exercise, together with the fit of Eq. 3 to the data in order to estimate k_{PCr}. Oxidative capacity of the TA muscle (Q_{max}) was measured at 0.69 mM ATP s^{-1}.

Table 1

Apparent T_1 values in different muscles of the lower leg of the recruited volunteers (mean ± SD).

	TA	TP	P	S	GL	GM
3T	5.90 ± 0.27	6.06 ± 0.22	5.84 ± 0.31	5.76 ± 0.33	5.92 ± 0.15	5.83 ± 0.22
7T	3.55 ± 0.08	3.63 ± 0.10	3.66 ± 0.07	3.52 ± 0.14	3.57 ± 0.15	3.48 ± 0.09

Table 2

PCr concentration (in mM) in the muscles of the lower leg measured at 3T and 7T

	TA		TP		P		S		GL		GM	
	3T	**7T**	**3T**	**7T**	**3T**	**7T**	**3T**	**7T**	**3T**	**7T**	**3T**	**7T**
Vol.1	31.2	32.2	30.5	30.3	30.2	31.1	29.2	31.8	32.7	32.9	30.5	30.3
Vol.2	34.1	32.6	32.5	33.7	32.5	31.8	33.1	34.1	31.5	31.2	32.1	33..3
Vol.3	27.2	28.2	27.3	28.1	28.9	28.5	26.9	27.9	27.7	27.5	28.0	28.6
Vol.4	32.3	31.1	32.3	32.8	30.8	31.3	31.1	32.2	33.7	32.8	33.3	32.8
Vol.5	34.5	33.8	34.8	33.5	33.9	33.2	32.0	33.5	33.1	32.9	34.8	34.2
Vol.6	25.7	24.5	25.3	24.9	24.7	25.1	24.8	25.2	25.3	26.1	25.8	25.5
Vol.7	27.3	28.9	28.1	27.2	27.9	27.5	28.1	27.8	28.5	28.2	29.1	28.5
Vol.8	25.5	24.5	25.2	25.3	24.7	24.5	24.1	24.5	25.5	24.8	25.1	24.9
Vol.9	29.4	30.2	28.5	29.8	29.5	29.7	28.5	29.5	28.3	29.2	28.7	29.1
Mean	29.7	29.6	29.4	29.5	29.2	29.2	28.6	29.6	29.6	29.5	29.7	29.2
SD	3.5	3.4	3.3	3.4	3.1	3.0	3.1	3.5	3.2	3.1	3.3	3.2

Magn Reson Med. Author manuscript; available in PMC 2014 December 01.